

Atomic ensemble-assisted ground-state cooling of a rotating mirror in a triple Laguerre–Gaussian cavity

Xiaoxuan Li(李晓璇), Junfei Chen(陈骏飞), and Qingxia Mu(穆青霞)

Citation: Chin. Phys. B, 2026, 35 (**1**): 014207. DOI: 10.1088/1674-1056/ade386
http://cpb.iphy.ac.cn; http://iopscience.iop.org/cpb

What follows is a list of articles you may be interested in

Coherent feedback ground-state cooling of mechanical resonators assisted by a quantum well

Qinghong Liao(廖庆洪), Songyun Ouyang(欧阳嵩沄), Shaoping Cheng(程绍平), and Yiping Cheng(程依萍)
Chin. Phys. B, 2025, 34 (**4**): 044202. DOI: 10.1088/1674-1056/adb266

Entangling two levitated charged nanospheres through Coulomb interaction

Guoyao Li(李国耀) and Zhangqi Yin(尹璋琦)
Chin. Phys. B, 2024, 33 (**7**): 074205. DOI: 10.1088/1674-1056/ad3229

Ground-state cooling based on a three-cavity optomechanical system in the unresolved-sideband regime

Jing Wang(王婧)
Chin. Phys. B, 2021, 30 (**2**): 024204. DOI: 10.1088/1674-1056/abc159

Double-passage mechanical cooling in a coupled optomechanical system

Qing-Xia Mu(穆青霞), Chao Lang(郎潮), Wen-Zhao Zhang(张闻钊)
Chin. Phys. B, 2019, 28 (**11**): 114206. DOI: 10.1088/1674-1056/ab48f1

Cavity optomechanics: Manipulating photons and phonons towards the single-photon strong coupling

Yu-long Liu(刘玉龙), Chong Wang(王冲), Jing Zhang(张靖), Yu-xi Liu(刘玉玺)
Chin. Phys. B, 2018, 27 (**2**): 024204. DOI: 10.1088/1674-1056/27/2/024204

Atomic ensemble-assisted ground-state cooling of a rotating mirror in a triple Laguerre–Gaussian cavity

Xiaoxuan Li(李晓璇), Junfei Chen(陈骏飞), and Qingxia Mu(穆青霞)†

Mathematics and Physics Department, North China Electric Power University, Beijing 102206, *China*

(Received 12 April 2025; revised manuscript received 7 June 2025; accepted manuscript online 11 June 2025)

We propose a novel cooling protocol within a triple-Laguerre–Gaussian cavity optomechanical system, which is designed to suppress the thermal vibrations of a rotating mirror to reach its quantum ground state. The system incorporates two auxiliary cavities and an atomic ensemble coupled to a Laguerre–Gaussian rotational cavity. By carefully selecting system parameters, the cooling process of the rotating mirror is significantly enhanced, while the heating process is effectively suppressed, enabling efficient ground-state cooling even in the unresolved sideband regime. Compared to previous works, our scheme reduces the stringent restrictions on auxiliary systems, making it more experimentally feasible under broader parameter conditions. These findings provide a robust approach for achieving ground-state cooling in mechanical resonators.

Keywords: triple Laguerre–Gaussian cavity, rotating mirror, ground-state cooling, atomic ensemble, rotational dynamics

PACS: 42.60.Da, 42.50.Nn, 03.65.Yz

DOI: 10.1088/1674-1056/ade386 **CSTR:** 32038.14.CPB.ade386

1. Introduction

Mechanical resonators, acting as a bridge between the classical and quantum realms, have attracted significant interest in the fields of quantum physics and nanotechnology. In particular, cavity optomechanical systems, which couple mechanical resonators with optical fields, enable the study of interactions between light and mechanical motion induced by radiation pressure.[1–5] This interaction has given rise to many fascinating phenomena,[6–10] showing the important role that cavity optomechanical systems play in both fundamental research and practical applications. For instance, it provides a unique platform for studying macroscopic quantum entanglement,[11–15] mechanical squeezing,[16,17] and macroscopic quantum superposition.[18–20] In addition, it allows for precise measurement of electrical charge,[21] environmental temperature,[22] and mass sensing improvement,[23] as well as the development of single-photon sources[24] and single-phonon sources.[25]

To realize nonclassical state preparation, quantum manipulation, and quantum measurement of mechanical resonators, it is essential to suppress environmental thermal noise by cooling macroscopic resonators to their vibrational ground state through coherent optomechanical interactions.[26–29] Therefore, achieving ground-state cooling with steady-state phonon number below 1, has become a central topic in optomechanical system.[28,29] So far, numerous theoretical and experimental methods for cooling mechanical resonators to their ground state have been extensively studied.[30–39] These include pure cryogenic cooling,[33] sideband cooling,[34,35] and feedback cooling,[36] among others. While sideband cooling remains the predominant technique in optomechanical manipulation, satisfying the resolved sideband regime requirements proves experimentally demanding in typical experimental optomechanical systems due to inherent limitations of optomechanical cooperativity.[37] As a result, much attention has turned to developing effective ground state cooling approaches in the unresolved sideband regime.[38,39] In this regime, the cavity decay rate needs to be significantly higher than the mechanical resonator's frequency.

A particularly promising strategy in this regime is assisted cooling, where additional quantum systems, such as atomic ensemble[40] or auxiliary cavity[41] is introduced to modify the optical response and enhance cooling while suppressing heating. Novel methods have been developed, including the auxiliary-cavity-mode technique, which allows for concurrent ground-state cooling of two mechanical modes that are degenerate or nearly degenerate,[42] or attaching an atomic ensemble and a cavity to the optomechanical system.[43] These methods illustrate the potential of assisted cooling to overcome the challenges of the unresolved sideband regime, offering promising solutions for achieving ground state cooling.

Recently, a Laguerre–Gaussian rotational-cavity optomechanical system was introduced, where two spiral phase elements act as cavity mirrors and enable orbital angular mo-

†Corresponding author. E-mail: qingxiamu@ncepu.edu.cn

© 2026 Chinese Physical Society and IOP Publishing Ltd. All rights, including for text and data mining, AI training, and similar technologies, are reserved.

mentum exchange.[44] Laguerre–Gaussian spiral phase systems, known for their distinctive optorotational interactions, have attracted considerable attention and spurred a range of applications, including quantum entanglement,[45,46] optomechanically induced transparency,[47,48] and ground-state cooling.[49–51] Unlike traditional optomechanical systems, the Laguerre–Gaussian rotational-cavity relies on rotational motion to couple with the optical field, potentially offering new prospects for achieving ground-state cooling. In particular, recent experiment demonstrate that high-intensity, high-purity, and broadband Laguerre–Gaussian modes can be generated using a Janus optical parametric oscillator.[52]

Drawing on existing research, we present a method for reducing the thermal motion of a rotating mirror to its quantum ground state within a triple Laguerre–Gaussian cavity. By incorporating a two-level atomic ensemble into the main optomechanical cavity and carefully adjusting auxiliary cavity parameters and atomic ensemble coupling conditions, the approach achieves enhanced cooling performance. In this paper, the appended cavity fields alter the channels of quantum interference effects, thereby providing our system with a greater number of tunable parameters to more effectively modulate the cooling performance. Compared with the earlier work in Ref. [51], a distinct advantage of our scheme is that the net cooling rate of the rotational mirror becomes larger when the second auxiliary cavity is introduced. This improvement arises from the additional quantum interference path introduced by the second auxiliary cavity, which further suppresses heating and enhances cooling. Moreover, the proposed scheme demonstrates the ability to suppress steady-state phonon number to approach zero under a broader range of system parameters. We also discuss the impact of each parameter on cooling effect, which offers valuable insights for the study of the physical properties of multi-Laguerre–Gaussian cavity optomechanical systems.

The analytical framework of this study is outlined as follows. Section 2 presents the system model and derivation of the effective Hamiltonian. Section 3 calculates the optical noise spectrum and final phonon number, also analyzing the impact of system parameters on the spectrum and optimal cooling conditions. Section 4 concludes the work.

2. Model and Hamiltonian

The system studied comprises three fixed mirrors (FM) and a rotating mirror (RM), creating a triple-Laguerre–Gaussian optomechanical system as depicted in Fig. 1. The RM mounted on a support S rotates around the Z_2 axis with an angular frequency ω_ϕ. In the absence of laser radiation, it maintains an equilibrium position $\phi_0 = 0$. When the angular deviation from its equilibrium position is sufficiently small, the RM's vibration can be considered as simple harmonic oscillation. The partially transparent input coupler FM_1 together with the perfectly reflective RM forms cavity 1, in which a two-level atomic ensemble is coupled. Meanwhile, FM_1 together with the perfectly reflective mirrors FM_2 and FM_3 establishes cavity 2 and cavity 3, respectively. In the absence of reflection, a Gaussian beam (G) with vanishing topological charge ($l = 0$) impinges on FM_1. Due to the opposite winding directions on its two sides, FM_1 allows the beam to pass through from either side without altering its topological charge.[53] As a result, the beam retains a zero topological charge upon transmission through FM_1 and drives the optical modes in cavity 1. After undergoing phase modulation at the RM, a topological charge of $+2l$ is added and then the beam returns to FM_1. At this point, a mode with zero charge is generated and enters cavity 2. Reflected from FM_2, the beam again acquires a topological charge of $+2l$. When it returns to FM_1, the transmitted beam with a charge of $+2l$ drives cavity 3. The topological charge reflected from FM_3 gives a mode with charge zero and returns to FM_1. Treating the RM as a thin disk, its mass and radius are defined as m and r, respectively. When it rotates around the Z_2 axis, the moment of inertia is easily obtained as $I = mr^2/2$. Since the RM is a torsion pendulum, it will necessarily vibrate when it rotates.

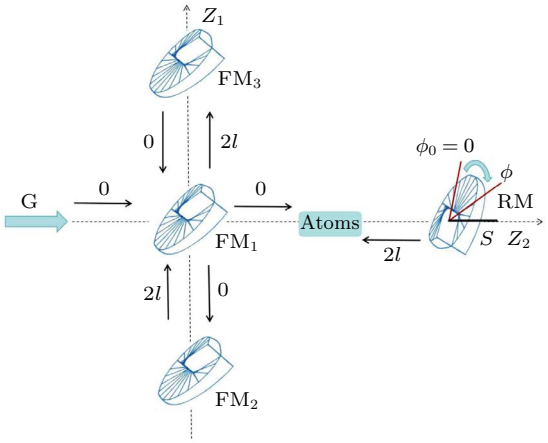


Fig. 1. Configuration diagram of a triple-Laguerre–Gaussian optomechanical setup.

Our analysis focuses on the mechanical effects of Laguerre–Gaussian beams interacting with the rotating mirror (RM). Laguerre–Gaussian beams possess not only spin angular momentum but also orbital angular momentum. Experimental studies demonstrate that orbital angular momentum transfer mechanisms in Laguerre–Gaussian modes induce rotational dynamics across microscopic particles[54] and Bose–Einstein condensates. Within the Bose–Einstein condensate, Laguerre–Gaussian beams can generate vortices.[55] These experiments have proven that Laguerre–Gaussian beams can

have a significant mechanical effect on macroscopic objects. When the Gaussian beam is incident on the cavity, it travels through the cavity with a traversal time of $2L/c$, where L is the length of cavity 1 and c is the speed of light. Each photon can convey a torque of $\xi_\phi = cl/L$ to the rotating mirror (RM). The Hamiltonian for the Laguerre–Gaussian optorotational system is expressed as ($\hbar = 1$),

$$\begin{aligned} H =& \sum_{j=1}^{3} \omega_{c_j} c_j^\dagger c_j + \sum_{i=1}^{N} (\omega_e |e\rangle_i\langle e| + \omega_g |g\rangle_i\langle g|) \\ &+ L_z^2/2I + (I\omega_\phi^2 \phi^2)/2 + J_{12}(c_1^\dagger c_2 + c_2^\dagger c_1) \\ &+ J_{13}(c_1^\dagger c_3 + c_3^\dagger c_1) + \sum_{i=1}^{N} g(c_1 |e\rangle_i\langle g| + c_1^\dagger |g\rangle_i\langle e|) \\ &- \xi_\phi \phi c_1^\dagger c_1 + \mathrm{i}(E_l c_1^\dagger \mathrm{e}^{-\mathrm{i}\omega_l t} - E_l^* c_1 \mathrm{e}^{\mathrm{i}\omega_l t}). \end{aligned} \tag{1}$$

The first two terms in Eq. (1) describe the non-interacting Hamiltonians for the j-th cavity mode and the atomic ensemble, respectively. Here, c_j ($c_j^\dagger$) represents the bosonic annihilation (creation) operator associated with three distinct cavity modes, characterized by eigenfrequencies ω_{cj} and dissipation rates κ_j. The parameters ω_g and ω_e correspond to the frequencies of the ground state $|g\rangle_i$ and the excited state $|e\rangle_i$, respectively. The third (fourth) term constitutes the RM's Hamiltonian, where L_z denotes the angular momentum and ϕ represents the angular displacement, satisfying the commutation relation $[L_z, \phi] = -\mathrm{i}\hbar$. The fifth (sixth) term formulates the interaction Hamiltonian between cavity modes c_1 and c_2 (c_3), with J_{12} and J_{13} being the corresponding coupling strengths. The seventh term denotes the interaction of the cavity field c_1 with the atomic ensemble, characterized by a coupling constant g. The photon-angular momentum exchange mechanism, namely optorotational coupling, between the cavity mode c_1 and RM is encapsulated in the eighth term. The final term of the Hamiltonian describes the coherent optical input to cavity mode c_1, driven at frequency ω_l with an amplitude of $|E_l| = \sqrt{2Pk_1/\hbar\omega_l}$, where P denotes the power of the input laser. In practice, fluctuations in the driving laser, such as amplitude and phase noise, can affect the quantum behavior of optomechanical systems.[56,57] With currently available stabilized lasers, the amplitude noise of the driving field can be neglected.[57] A recent study[58] demonstrates that laser phase noise can be suppressed through various techniques, such as destructive-interference schemes,[59] parametric amplification,[60] fiber-loop delay line interferometers,[61] and others. Therefore, in principle, laser phase noise can be effectively suppressed by employing these methods. Especially for our scheme, the impact of laser phase noise can be reduced by additional filtering cavities, as shown in Ref. [62]. More importantly, our triple Laguerre–Gaussian cavity combined with an atomic ensemble introduces additional destructive interference channels that can effectively suppress laser phase noise. As a result, the effect of laser noise is not included in our analysis.

We can define

$$\phi = \sqrt{\frac{\hbar}{2I\omega_\phi}}(b^\dagger + b), \quad L_z = \mathrm{i}\sqrt{\frac{I\hbar\omega_\phi}{2}}(b^\dagger - b), \tag{2}$$

where b and $b^\dagger$ denote the annihilation and creation operators for the rotating mirrors, respectively. Therefore,the Hamiltonian can be further simplified to

$$\begin{aligned} H' =& \sum_{j=1}^{3} \omega_{c_j} c_j^\dagger c_j + \sum_{i=1}^{N} (\omega_e |e\rangle_i\langle e| + \omega_g |g\rangle_i\langle g|) \\ &+ \omega_\phi b^\dagger b + J_{12}(c_1^\dagger c_2 + c_2^\dagger c_1) + J_{13}(c_1^\dagger c_3 \\ &+ c_3^\dagger c_1) + \sum_{i=1}^{N} g(c_1 |e\rangle_i\langle g| + c_1^\dagger |g\rangle_i\langle e|) \\ &- G c_1^\dagger c_1 (b^\dagger + b) + \mathrm{i}(E_l c_1^\dagger \mathrm{e}^{-\mathrm{i}\omega_l t} - E_l^* c_1 \mathrm{e}^{\mathrm{i}\omega_l t}), \end{aligned} \tag{3}$$

where the coupling coefficient is defined as $G = \frac{cl}{L}\sqrt{\hbar/2I\omega_\phi}$. It should be noted that the topological charge l has a direct impact on the coupling coefficient. A moderate increase in l can enhance the coupling and thereby influencing the cooling performance.[50] In our scheme, we set $l = 100$,[63] which is experimentally feasible and ensures that the system operates in the weak coupling regime.

We consider that the majority of atoms are prepared in there ground states, thereby fulfilling the weak excitation condition. Under this condition, the atomic ensemble can be effectively treated as a bosonic mode described by the collective operator $a = \frac{1}{\sqrt{N}}\sum_{i=1}^{N} |g\rangle_i\langle e|$,[64] which obeys the commutation relation $[a, a^\dagger] = 1$. In the rotating frame aligned with the driving laser frequency ω_l, the Hamiltonian is given by

$$\begin{aligned} H'' =& \sum_{j=1}^{3} \Delta_j c_j^\dagger c_j + \Delta_4 a^\dagger a + \omega_\phi b^\dagger b + J_{12}(c_1^\dagger c_2 \\ &+ c_2^\dagger c_1) + J_{13}(c_1^\dagger c_3 + c_3^\dagger c_1) + g'(c_1 a^\dagger + c_1^\dagger a) \\ &- G c_1^\dagger c_1 (b^\dagger + b) + \mathrm{i}(E_l c_1^\dagger - E_l^* c_1), \end{aligned} \tag{4}$$

where $\Delta_j = \omega_j - \omega_l$ and $\Delta_4 = \omega_{eg} - \omega_l$ are the detunings from the driving field for the three cavity modes and atomic ensemble, respectively, with ω_{eg} being the eigenfrequency of the atoms. The effective coupling strength $g' = \sqrt{N}g$ characterizes the collectively enhanced interaction between the cavity mode and the atomic ensemble. Taking into account the damping and noises of the environment, the system evolution is governed by quantum Langevin master equations of the form

$$\begin{aligned} \dot{c}_1 =& -(\mathrm{i}\Delta_1 + k_1)c_1 + \mathrm{i}G c_1 (b^\dagger + b) - \mathrm{i}J_{12}c_2 \\ &- \mathrm{i}J_{13}c_3 - \mathrm{i}g' a + E_l + \sqrt{2k_1}c_{1,\mathrm{in}}(t), \\ \dot{c}_2 =& -(\mathrm{i}\Delta_2 + k_2)c_2 - \mathrm{i}J_{12}c_1 + \sqrt{2k_2}c_{2,\mathrm{in}}(t), \\ \dot{c}_3 =& -(\mathrm{i}\Delta_3 + k_3)c_3 - \mathrm{i}J_{13}c_1 + \sqrt{2k_3}c_{3,\mathrm{in}}(t), \\ \dot{a} =& -(\mathrm{i}\Delta_4 + \gamma_\mathrm{a})a - \mathrm{i}g' c_1 + \sqrt{2\gamma_\mathrm{a}}a_\mathrm{in}(t), \\ \dot{b} =& -(\mathrm{i}\omega_\phi + \gamma_\mathrm{m})b + \mathrm{i}G c_1^\dagger c_1 + \sqrt{2\gamma_\mathrm{m}}b_\mathrm{in}(t), \end{aligned} \tag{5}$$

where $\gamma_{\rm a}$ and $\gamma_{\rm m}$ are the decay rates of the atoms and the RM. The input noises $c_{j,\rm in}$ $(j=1,2,3)$, $a_{\rm in}$ and $b_{\rm in}$, associated respectively with the three cavity modes, the atomic ensemble, and the RM, satisfy the correlation functions

$$\begin{aligned}
&\langle c_{j,\rm in}(t)c_{j,\rm in}^{\dagger}(t')\rangle=\delta(t-t'),\quad \langle c_{j,\rm in}^{\dagger}(t)c_{j,\rm in}(t')\rangle=0,\\
&\langle a_{\rm in}(t)a_{\rm in}^{\dagger}(t')\rangle=\delta(t-t'),\quad \langle a_{\rm in}^{\dagger}(t)a_{\rm in}(t')\rangle=0,\\
&\langle b_{\rm in}(t)b_{\rm in}^{\dagger}(t')\rangle=(n_{\rm th}+1)\delta(t-t'),\\
&\langle b_{\rm in}^{\dagger}(t)b_{\rm in}(t')\rangle=n_{\rm th}\delta(t-t'),
\end{aligned}\tag{6}$$

here $n_{\rm th}=1/\left(\mathrm{e}^{\hbar\omega_\phi/k_{\rm B}T}-1\right)$ denotes the thermal noise number at the environment temperature T.

When the system is strongly driven, it is appropriate to apply the standard linearization technique, expressing each operator as a combination of a steady-state component and a small fluctuation term: $c_i=\bar{c}_i+\delta c_i$ $(i=1,2,3)$, $a=\alpha+\delta a$, $b=\beta+\delta b$. With the above Langevin equations, we can obtain the steady-state values as

$$\begin{aligned}
\bar{c}_1 &= \frac{E_l}{\mathrm{i}\Delta_1'+\kappa_1+\frac{J_{12}^2}{\mathrm{i}\Delta_2+\kappa_2}+\frac{J_{13}^2}{\mathrm{i}\Delta_3+\kappa_3}+\frac{g'^2}{\mathrm{i}\Delta_4+\gamma_{\rm a}}},\\
\bar{c}_2 &= -\frac{\mathrm{i}J_{12}\bar{c}_1}{\mathrm{i}\Delta_2+\kappa_2},\quad \bar{c}_3=-\frac{\mathrm{i}J_{13}\bar{c}_1}{\mathrm{i}\Delta_3+\kappa_3},\\
\alpha &= -\frac{ig'\bar{c}_1}{\mathrm{i}\Delta_4+\gamma_{\rm a}},\quad \beta=\frac{\mathrm{i}G|\bar{c}_1|^2}{\mathrm{i}\omega_\phi+\gamma_{\rm m}}.
\end{aligned}\tag{7}$$

Since the average value of the physical quantity typically surpasses its fluctuations, higher-order nonlinear terms can be neglected. This allows us to derive the linearized quantum Langevin equations (with the fluctuation operator symbol "δ" omitted for notational brevity)

$$\begin{aligned}
\dot{c}_1 &= -(\mathrm{i}\Delta_1'+k_1)c_1+\mathrm{i}G'(b^{\dagger}+b)-\mathrm{i}J_{12}c_2\\
&\quad -\mathrm{i}J_{13}c_3-\mathrm{i}g'a+\sqrt{2k_1}c_{1,\rm in}(t),\\
\dot{c}_2 &= -(\mathrm{i}\Delta_2+k_2)c_2-\mathrm{i}J_{12}c_1+\sqrt{2k_2}c_{2,\rm in}(t),\\
\dot{c}_3 &= -(\mathrm{i}\Delta_3+k_3)c_3-\mathrm{i}J_{13}c_1+\sqrt{2k_3}c_{3,\rm in}(t),\\
\dot{a} &= -(\mathrm{i}\Delta_4+\gamma_{\rm a})a-\mathrm{i}g'c_1+\sqrt{2\gamma_{\rm a}}a_{\rm in}(t),\\
\dot{b} &= -(\mathrm{i}\omega_\phi+\gamma_{\rm m})b+\mathrm{i}G'(c_1^{\dagger}+c_1)+\sqrt{2\gamma_{\rm m}}b_{\rm in}(t).
\end{aligned}\tag{8}$$

The effective linearized Hamiltonian of the system then takes the form

$$\begin{aligned}
H_{\rm eff} &= \Delta_1'c_1^{\dagger}c_1+\sum_{j=2}^{3}\Delta_jc_j^{\dagger}c_j+\Delta_4a^{\dagger}a+\omega_\phi b^{\dagger}b\\
&\quad +J_{12}(c_1^{\dagger}c_2+c_2^{\dagger}c_1)+J_{13}(c_1^{\dagger}c_3+c_3^{\dagger}c_1)\\
&\quad +g'(c_1a^{\dagger}+c_1^{\dagger}a)-G'(c_1^{\dagger}+c_1)(b^{\dagger}+b),
\end{aligned}\tag{9}$$

where $\Delta_1'=\Delta_1-G(\beta+\beta^*)$ is the modified detuning induced by the driving field and $G'=\bar{c}_1G$ is the linearized optorotational coupling strength.

3. Ground-state cooling of RM

3.1. The fluctuation spectrum and phonon number equations

In this section, we proceed to calculate the optical noise spectrum and ascertain the final phonon number. In the regime of weak optomechanical coupling where $G'\ll\omega_\phi$, the optorotational interaction becomes negligible, but the influence of the atomic ensemble can no longer be disregarded. As a result, the Hamiltonian that determines the fluctuation spectrum can be rewritten as

$$\begin{aligned}
H_{\rm op} &= \Delta_1'c_1^{\dagger}c_1+\sum_{j=2}^{3}\Delta_jc_j^{\dagger}c_j+\Delta_4a^{\dagger}a+J_{12}(c_1^{\dagger}c_2\\
&\quad +c_2^{\dagger}c_1)+J_{13}(c_1^{\dagger}c_3+c_3^{\dagger}c_1)+g'(c_1a^{\dagger}+c_1^{\dagger}a).
\end{aligned}\tag{10}$$

The Langevin equations for the cavity-ensemble system in the frequency domain are given by

$$\begin{aligned}
-\mathrm{i}\omega c_1(\omega) &= -(\mathrm{i}\Delta_1'+k_1)c_1(\omega)-\mathrm{i}J_{12}c_2(\omega)\\
&\quad -\mathrm{i}J_{13}c_3(\omega)-\mathrm{i}g'a(\omega)+\sqrt{2k_1}c_{1,\rm in}(\omega),\\
-\mathrm{i}\omega c_2(\omega) &= -(\mathrm{i}\Delta_2+k_2)c_2(\omega)-\mathrm{i}J_{12}c_1(\omega)\\
&\quad +\sqrt{2k_2}c_{2,\rm in}(\omega),\\
-\mathrm{i}\omega c_3(\omega) &= -(\mathrm{i}\Delta_3+k_3)c_3(\omega)-\mathrm{i}J_{13}c_1(\omega)\\
&\quad +\sqrt{2k_3}c_{3,\rm in}(\omega),\\
-\mathrm{i}\omega a(\omega) &= -(\mathrm{i}\Delta_4+\gamma_{\rm a})a(\omega)-\mathrm{i}g'c_1(\omega)\\
&\quad +\sqrt{2\gamma_{\rm a}}a_{\rm in}(\omega).
\end{aligned}\tag{11}$$

By analyzing the optically torsional force on the RM, one can clearly observe the system's cooling and heating effects within the optical force spectrum. In the linearized Hamiltonian Eq. (9), the effective optically torsional force on the RM is given by $F=c_1+c_1^{\dagger}$, and the fluctuation spectrum of F can be derived as $S_{\rm F}(\omega)=\int_{-\infty}^{\infty}\mathrm{d}t\,\mathrm{e}^{\mathrm{i}\omega t}\langle F(t)F(0)\rangle$. The result is as follows:

$$\begin{aligned}
S_{\rm F}(\omega) &= 2|X(\omega)|^2\left[|J_{12}X_2(\omega)|^2k_2\right.\\
&\quad \left.+|J_{13}X_3(\omega)|^2k_3+|g'X_4(\omega)|^2\gamma_{\rm a}+k_1\right],
\end{aligned}\tag{12}$$

where

$$\begin{aligned}
\frac{1}{X_1(\omega)} &= \mathrm{i}(\Delta_1'-\omega)+\kappa_1,\\
\frac{1}{X_2(\omega)} &= \mathrm{i}(\Delta_2-\omega)+\kappa_2,\\
\frac{1}{X_3(\omega)} &= \mathrm{i}(\Delta_3-\omega)+\kappa_3,\\
\frac{1}{X_4(\omega)} &= \mathrm{i}(\Delta_4-\omega)+\gamma_{\rm a},\\
X(\omega) &= \frac{1}{\frac{1}{X_1(\omega)}+X_2(\omega)J_{12}^2+X_3(\omega)J_{13}^2+g'^2X_4(\omega)}.
\end{aligned}\tag{13}$$

Here, $X(\omega)$ quantifies the system's total response function, where $X_j(\omega)$ $(j=1$–$4)$ denote the response functions of the active cavity, the two auxiliary cavities, and the atomic ensemble, respectively. Based on Fermi's golden rule,[65,66] we

derive the following expression, which yields the final mean phonon number of the RM's steady state

$$N_{\rm f} = \frac{\gamma_{\rm m} n_{\rm th} + \Gamma_{\rm c} n_{\rm c}}{\gamma_{\rm m} + \Gamma_{\rm c}}, \tag{14}$$

where

$$\begin{aligned} n_{\rm c} &= \frac{S_{\rm F}(-\omega_\phi)}{S_{\rm F}(\omega_\phi) - S_{\rm F}(-\omega_\phi)}, \\ \Gamma_{\rm c} &= G'^2[S_{\rm F}(\omega_\phi) - S_{\rm F}(-\omega_\phi)]. \end{aligned} \tag{15}$$

As can be seen from Eq. (14), the final phonon number is primarily determined by four parameters: $\gamma_{\rm m}$, $n_{\rm th}$, $\Gamma_{\rm c}$, and $n_{\rm c}$. In this framework, $\Gamma_{\rm c}$ denotes the net cooling rate, while $n_{\rm c}$ represents the quantum limit of cooling. $S_{\rm F}(\omega_\phi)$ and $S_{\rm F}(-\omega_\phi)$ correspond to the cooling rate and heating rate of the mechanical mode (RM), respectively. When the coupling between the mechanical mode and the thermal bath is disregarded, specifically as $n_{\rm th} \to 0$, the final phonon number $N_{\rm f}$ tends towards the quantum limit $n_{\rm c}$. This behavior highlights that the final phonon number remains bounded from below by a nonzero value. Therefore, to achieve a smaller $N_{\rm f}$, it is necessary to have a larger value of $\Gamma_{\rm c}$ while keeping $n_{\rm c}$ as small as possible. As indicated by Eq. (15), $\Gamma_{\rm c}$ and $n_{\rm c}$ are governed by the spectral components $S_{\rm F}(\omega_\phi)$ and $S_{\rm F}(-\omega_\phi)$ of the optical noise spectrum. Consequently, to achieve ground-state cooling of the mechanical oscillator, it is essential to enhance the cooling process while simultaneously suppress the heating process.

Table 1. The possible experimental parameters.[63]

Number	Parameter	Description	Value	Units
1	L	cavity length	0.245	mm
2	λ	laser wavelength	810	nm
3	ω_ϕ	rotating mirror frequency	$2\pi \times 10$	MHz
4	m	rotating mirror mass	100	ng
5	r	rotating mirror radius	10	μm
6	$Q_{\rm m}$	mechanical quality factor	10^5	
7	l	orbital angular momentum	100	$\hbar$
8	g'	coupling strength between atoms and cavity	$2\pi \times 10$	MHz
9	$\gamma_{\rm a}$	spontaneous decay rate of atom	$2\pi \times 5$	MHz
10	T	environment temperature	150	mK
11	Δ/ω_ϕ	normalized laser detuning	–1	

3.2. Analysis of the optical force spectrum $S_{\rm F}(\omega)$

As previously mentioned, the resolved sideband regime has been extensively explored in the context of sideband cooling theory. However, due to the strict requirements on experimental conditions, our study focuses on the more challenging task of cooling within the unresolved sideband regime. To optimize the cooling performance, we then analyze how the fluctuation spectrum $S_{\rm F}(\omega)$ depends on the key parameters, including the inter-cavity coupling strength, cavity-ensemble coupling, and the effective detunings. For maximum suppression of heating effects, the spectral minimum occurs at $\Delta_2 = \Delta_3 = \Delta_4 = \Delta = -\omega_\phi$.

As depicted in Fig. 2, the optical force fluctuation spectrum $S_{\rm F}(\omega)$ versus the frequency ω is plotted for different coupling strengths of the auxiliary cavities. The decay rates of the three cavities are chosen as $\kappa_1 = 1.5\omega_\phi$, $\kappa_2 = 2\omega_\phi$, and $\kappa_3 = 1.5\omega_\phi$, respectively, which is beyond the resolved sideband regime. It can be observed that when a single cavity is coupled, *i.e.*, $J_{12} = \omega_\phi$, $J_{13} = 0$, the value of the optical noise spectrum at $\omega = -\omega_\phi$ decreases than the case of $J_{12} = J_{13} = 0$. Furthermore, when both cavities are coupled, the dip in the optical noise spectrum decreases even more significantly, indicating that the suppression of heating is more effective.

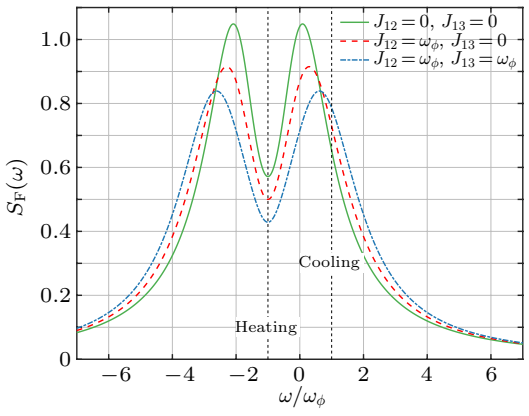


Fig. 2. The $S_{\rm F}(\omega)$ (in arb. units) versus ω for different values of auxiliary cavity coupling strengths. Here, $\kappa_1 = 1.5\omega_\phi$, $\kappa_2 = 2\omega_\phi$, $\kappa_3 = 1.5\omega_\phi$, and $\Delta_1' = -\omega_\phi$. The other parameters are chosen as those in Table 1.

In Fig. 3, we plot the fluctuation spectrum $S_{\rm F}(\omega)$ for different cavity-ensemble couplings g'. In the absence of the atomic ensemble ($g' = 0$), although the fluctuation spectrum splits into two narrower peaks with a dip in the middle, the suppression of heating is not optimal. However, when considering the atomic ensemble, the thermal effect can be strongly suppressed as the coupling increases. The reason for this phenomenon is that in hybrid quantum systems, the excitation

pathways experience quantum interference due to the coupling with auxiliary systems.[67] Since our scheme involves coupling to both the cavities and the atomic ensemble, there are more interference channels available in hybrid systems with multiple auxiliary systems, which allows for more effective suppression of transitions related to heating.

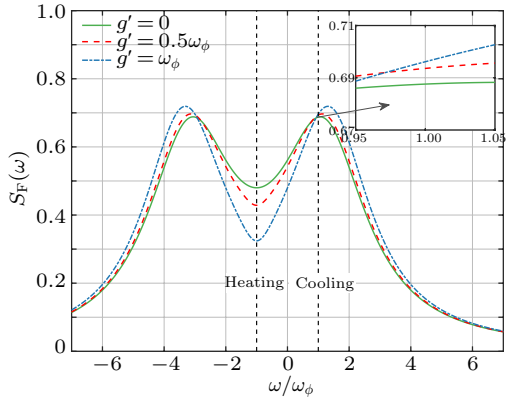


Fig. 3. The $S_F(\omega)$ (in arb. units) versus ω for different values of g'. Here, $J_{12}=2\omega_\phi$, $J_{13}=\omega_\phi$, and $\Delta_1'=-\omega_\phi$. The other parameters are chosen as those in Table 1.

To maximize the cooling process, we further investigate the influence of the coupling strengths and the effective detuning Δ_1' on the optical force spectrum $S_F(\omega)$. It should be noted that the appearance and width of the dip in the spectrum $S_F(\omega)$ can be understood from the perspective of dressed-state theory.[68] By diagonalizing the Hamiltonian in Eq. (10), we can determine the optimal values for the effective detuning and coupling strengths needed to attain the optimal cooling regime. The resulting diagonalized Hamiltonian is expressed as

$$H_d=\omega_-\tilde{a}_-^\dagger\tilde{a}_-+\omega_{01}\tilde{a}_{01}^\dagger\tilde{a}_{01}+\omega_{02}\tilde{a}_{02}^\dagger\tilde{a}_{02}+\omega_+\tilde{a}_+^\dagger\tilde{a}_+. \quad (16)$$

Here $\tilde{a}_{-,01,02,+}$ represent the collective annihilation operators, and $\omega_{-,01,02,+}$ are the eigenfrequencies of the diagonalized system. The dip of the fluctuation spectrum $S_F(\omega)$ occurs at $\omega_{01}=\omega_{02}=\Delta$, while the peaks are located at

$$\omega_\pm=\frac{\Delta_1'+\Delta}{2}\pm\sqrt{\left(\frac{\Delta_1'-\Delta}{2}\right)^2+g'^2+J_{12}^2+J_{13}^2}. \quad (17)$$

As mentioned before, if we set $\Delta=-\omega_\phi$, the minimum value of the fluctuation spectrum appears at $\omega=-\omega_\phi$, which suppressing the heating process effectively. By positioning the right peak at $\omega_+=+\omega_\phi$, we obtain the optimal cooling conditions as follows:

$$\Delta_1'=\omega_\phi-\frac{g'^2+J_{12}^2+J_{13}^2}{2\omega_\phi}. \quad (18)$$

If equation (18) is satisfied and the condition $\Delta=-\omega_\phi$ is met, the right peak is always at $+\omega_\phi$, and the dip occurs at $-\omega_\phi$, thereby the optimal cooling performance can be achieved. In the discussion of the following parameters, the optimal coupling strengths take values that satisfy this equation.

To investigate the effect of the auxiliary cavity dissipation, we present in Fig. 4 the fluctuation spectrum $S_F(\omega)$ for three different values of the caivity decay rate κ_2 as an example. We can observe that when k_2 decreases, the dip in the optical noise spectrum decreases and the right peak of the optical noise spectrum increases, which means the corresponding cooling rate Γ_c becomes larger. Therefore, it is also necessary to appropriately select κ_2 to achieve ideal ground-state cooling. Although we find that smaller values of k_2 are beneficial for ground-state cooling, some systems cannot meet the sideband-resolvable condition: $\kappa\ll\omega_\phi$. However, in our study, even when $\kappa_2(\kappa_3)>\omega_\phi$, the RM can still be successfully cooled to its ground state beyond the resolved sideband condition due to the contribution of the auxiliary systems.

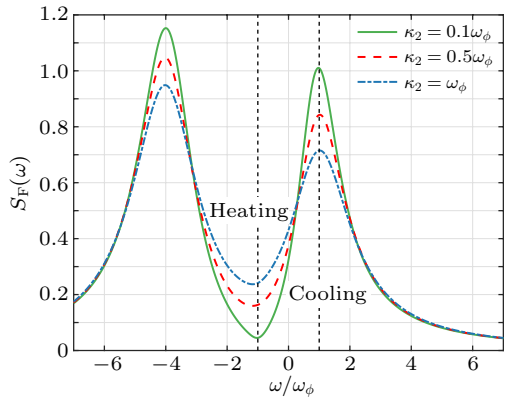


Fig. 4. The $S_F(\omega)$ (in arb. units) versus ω for different decay rates κ_2. Here, $J_{12}=2\omega_\phi$, $J_{13}=\omega_\phi$, and Δ_1' satisfies Eq. (18). The other parameters are chosen as those in Table 1.

The impact of the atomic ensemble's decay rate γ_a on the fluctuation spectrum is also analyzed. As shown in Fig. 5, the decay rate γ_a affects $S_F(\omega)$ in a similar way to κ_2. Specifically, for small values of γ_a, $S_F(-\omega)$ decreases while $S_F(\omega)$ increases, which is beneficial for cooling.

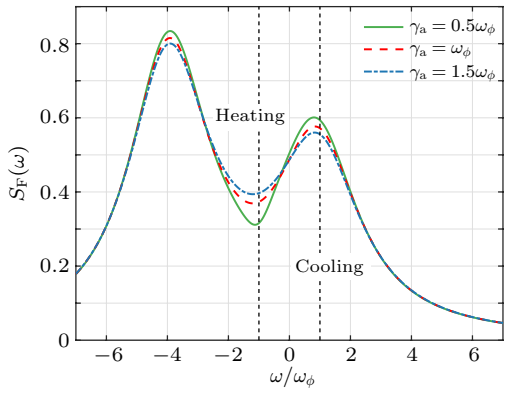


Fig. 5. The $S_F(\omega)$ (in arb. units) versus ω for different values of atomic ensemble γ_a. Here, $J_{12}=2\omega_\phi$, $J_{13}=\omega_\phi$, and Δ_1' satisfies Eq. (18). The other parameters are chosen as those in Table 1.

We then turn to the investigation of the cooling rate. In Fig. 6, we present the variation of the net cooling rate Γ_c with the decay rate κ_1. It is observed that Γ_c is lowest when there is no coupling to either the auxiliary cavity or the atomic ensemble. Introducing coupling to the auxiliary cavity or the atomic ensemble leads to an increase in Γ_c. When both the auxiliary cavity and the atomic ensemble are coupled to the system, Γ_c

increases significantly. It is worth noting that, with appropriate parameters, Γ_c is enhanced when both auxiliary cavities are present compared to the case of only one auxiliary cavity (as in Ref. [51]). This further confirms that the introduction of auxiliary systems can significantly enhance the cooling performance.

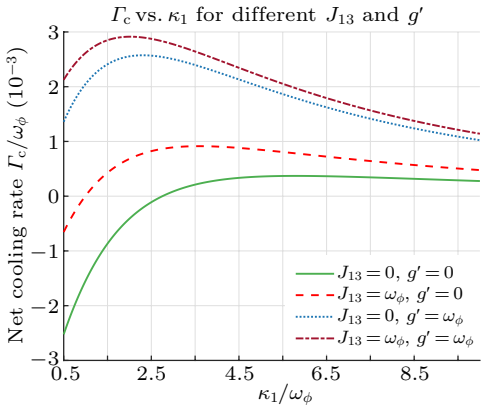


Fig. 6. The net cooling rate Γ_c (in arb. units) varies with the decay rate κ_1 for different coupling strengths J_{13} and g'. Here, $G'=0.2\omega_\phi$, $J_{12}=3\omega_\phi$, $\kappa_2=3\omega_\phi$, Δ_1' satisfies Eq. (18). The other parameters are chosen as those in Table 1.

3.3. Analysis of the photon number N_f

Based on the previous analysis, we now focus on the final mean phonon number N_f, a critical indicator for ground-state cooling, which must be reduced below 1.

In order to examine how the auxiliary cavities and the atomic ensemble affect the phonon number N_f, we plot N_f as a function of the coupling strengths J_{12} and J_{13} for $g'=0$ (Fig. 7(a)) and $g'=\omega_\phi$ (Fig. 7(b)). For any values of J_{12}, J_{13}, and g', the effective detuning Δ_1' satisfies the optimal cooling condition Eq. (18). The white line indicates the contour where $N_f=1$, meaning that ground-state cooling can be achieved within this region. As we can see, by adding the atomic ensemble, ground-state cooling becomes achievable over a much wider range of J_{12} and J_{13}. This is because coupling both the auxiliary cavities and the atomic ensemble to the system introduces additional quantum interference, leading to enhanced destructive interference that more effectively suppresses heating processes. Consequently, the desired cooling effect can be achieved by properly selecting the coupling strengths.

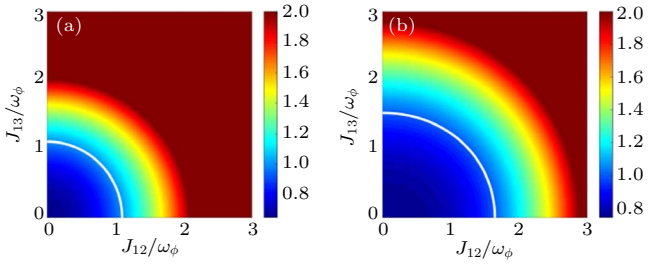


Fig. 7. The N_f versus J_{12} and J_{13} for (a) $g'=0$ and (b) $g'=\omega_\phi$. Here, $G'=0.2\omega_\phi$, $T=150$ mK implying $n_{th}=312$, and Δ_1' satisfies Eq. (18). The other parameters are chosen as those in Table 1.

To determine the reasonable range of the coupling strength g' and the atomic ensemble decay rate γ_a for achieving ideal ground-state cooling, we plot the final mean phonon number N_f as a function of g' and γ_a in Fig. 8. The critical value of the atomic ensemble decay rate is $\gamma_a\approx 1.13\omega_\phi$, corresponding to a coupling strength $g'\approx 4\omega_\phi$ in the strong coupling regime. Notably, even when the resolved sideband condition is not satisfied and the atomic ensemble decay rate is relatively large, ground-state cooling can still be achieved. At higher g', the cooling efficiency significantly improves, even for larger γ_a, demonstrating that strong coupling can effectively counterbalance higher dissipation.

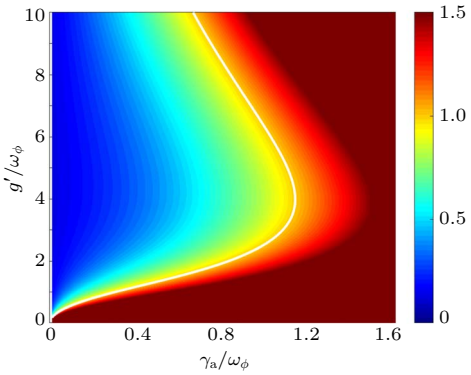


Fig. 8. The N_f versus γ_a and g'. Here, $G'=0.2\omega_\phi$, $J_{12}=2\omega_\phi$, $J_{13}=\omega_\phi$, and Δ_1' satisfies Eq. (18). The other parameters are chosen as those in Table 1.

In Fig. 9, we plot the phonon number N_f against the decay rates κ_1 and κ_2. Notably, even when κ_1 reaches $8\omega_\phi$, N_f remains below 1. Furthermore, N_f is still less than 1 even as κ_2 increases to $18\omega_\phi$. In contrast to traditional cooling schemes that strongly depend on the high-quality auxiliary cavity (i.e., a low κ_2). Such robustness against auxiliary-cavity dissipation, combined with the ability to achieve cooling in the unresolved sideband regime, highlights the experimental feasibility of our hybrid optorotational cooling scheme.

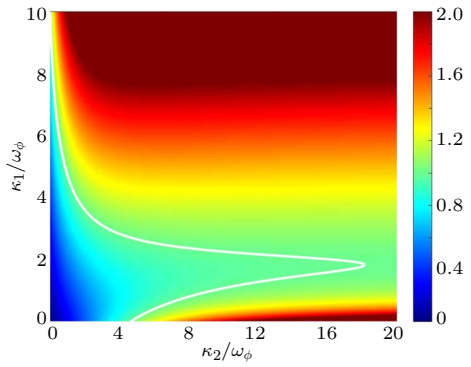


Fig. 9. The N_f versus κ_1 and κ_2. Here, $G'=0.2\omega_\phi$, $J_{12}=2\omega_\phi$, $J_{13}=\omega_\phi$, $g'=2\omega_\phi$, and Δ_1' satisfies Eq. (18). The other parameters are chosen as those in Table 1.

Figure 10 demonstrates how the phonon number N_f varies with the thermal bath phonon number n_{th} and cavity decay rate κ_1. The results demonstrate that, even with a large n_{th}, the final phonon number N_f can remain below 1 by appropriately

controlling the cavity dissipation rate. This emphasizes the robustness and experimental advantages of this cooling scheme in high-temperature or high-noise environments.

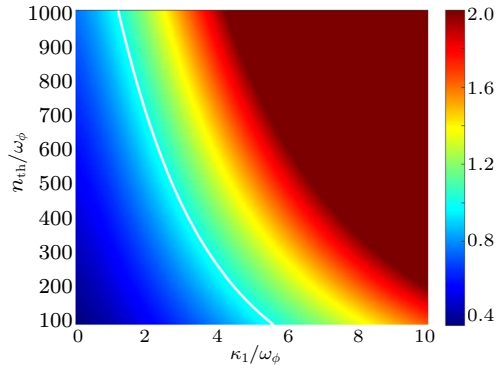


Fig. 10. The $N_{\rm f}$ versus κ_1 and $n_{\rm th}$. Here, $G' = 0.2\omega_\phi$, $J_{12} = 2\omega_\phi$, $J_{13} = \omega_\phi$, $g' = 2\omega_\phi$, and Δ_1' satisfies Eq. (18). The other parameters are chosen as those in Table 1.

Now, we proceed to discuss the experimental feasibility of the proposed system. As summarized in Table 1, we adopt parameters similar to those used in previous studies on Laguerre–Gaussian optomechanical systems.[51,58,63] Specifically, we take $\omega_\phi = 2\pi \times 10$ MHz, $L = 0.245$ mm, $r = 10$ μm, $m = 100$ ng. High-l Laguerre–Gaussian modes have been shown to be experimentally accessible using spiral phase elements.[69] Here, we set $l = 100$. Based on these parameters, the single-photon coupling strength is calculated to be $G \sim 2 \times 10^{-5}\omega_\phi$, confirming that the system is in the weak-coupling limit. Besides, the mechanical quality factor of RM is set to be $Q_{\rm m} = 10^5$, corresponding to a mechanical damping rate $\gamma_{\rm m} = 10^{-5}\omega_\phi$. Notably, mechanical oscillators with quality factor of $Q \sim 1.3 \times 10^5$, low effective mass of 25 ng, and a radius of 15 μm have been demonstrated,[70] which implies that the proposed scheme is feasible in experiment with current technology.

4. Conclusions

This paper presents a theoretical scheme for intracavity compression cooling of a rotating mirror based on a triple-Gaussian rotating cavity coupled with an atomic ensemble composite quantum system. These results indicate that the inclusion of an atomic ensemble can suppress the quantum back-action heating process, and the coupling of auxiliary cavities can significantly enhance the cooling efficiency, thereby optimizing the cooling process. Especially, compared with Ref. [51], our triple-cavity setup achieves a higher net cooling rate under appropriate parameters, due to the presence of the additional quantum interference path. Furthermore, by satisfying Eq. (18) and selecting appropriate coupling strengths, effective detuning quantities, and cavity field decay rates, the ideal cooling effect can be achieved. With the aid of the atomic ensemble, the restrictions on the auxiliary cavities in the composite system are reduced. This study has potential application value in achieving the quantum ground state of the rotating mirror and greatly promotes the research of various quantum phenomena in optorotational systems.

Acknowledgement

Project supported by the National Natural Science Foundation of China (Grant No. 62471180).

References

[1] Agarwal G S and Huang S 2010 *Phys. Rev. A* **81** 041803
[2] Wang T, Zheng M H, Bai C H, Wang D Y, Zhu A, Wang H and Zhang S 2018 *Annalen der Physik* **530** 1800228
[3] Yan X B 2020 *Phys. Rev. A* **101** 043820
[4] Verhagen E, Deléglise S, Weis S, Schliesser A and Kippenberg T J 2012 *Conference on Lasers and Electro-Optics* 2012 (Optica Publishing Group) p. JM1K.1
[5] Aspelmeyer M, Kippenberg T J and Marquardt F 2014 *Rev. Mod. Phys.* **86** 1391
[6] Maayani S, Dahan R, Kligerman Y, Moses E, Hassan A U, Jing H, Nori F, Christodoulides D N and Carmon T 2018 *Nature* **558** 569
[7] Li B, Huang R, Xu X, Miranowicz A and Jing H 2019 *Photon. Res.* **7** 630
[8] Jiang C, Song L N and Li Y 2018 *Phys. Rev. A* **97** 053812
[9] Bai C H, Wang D Y, Zhang S, Liu S and Wang H 2018 *Annalen der Physik* **531** 1800271
[10] Yan X B, Lu H L, Gao F and Yang L 2018 *Frontiers of Physics* **14** 52601
[11] Vitali D, Gigan S, Ferreira A, Böhm H R, Tombesi P, Guerreiro A, Vedral V, Zeilinger A and Aspelmeyer M 2007 *Phys. Rev. Lett.* **98** 030405
[12] Huang S and Agarwal G S 2009 *New J. Phys.* **11** 103044
[13] Liao J Q, Wu Q Q and Nori F 2014 *Phys. Rev. A* **89** 014302
[14] Li J, Haghighi I M, Malossi N, Zippilli S and Vitali D 2015 *New J. Phys.* **17** 103037
[15] Wang M, Lü X Y, Wang Y D, You J Q and Wu Y 2016 *Phys. Rev. A* **94** 053807
[16] Lü X Y, Liao J Q, Tian L and Nori F 2015 *Phys. Rev. A* **91** 013834
[17] Agarwal G S and Huang S 2016 *Phys. Rev. A* **93** 043844
[18] Ge W and Zubairy M S 2015 *Phys. Rev. A* **91** 013842
[19] Liao J Q and Tian L 2016 *Phys. Rev. Lett.* **116** 163602
[20] Hoff U B, Kollath-Bönig J, Neergaard-Nielsen J S and Andersen U L 2016 *Phys. Rev. Lett.* **117** 143601
[21] Zhang J Q, Li Y, Feng M and Xu Y 2012 *Phys. Rev. A* **86** 053806
[22] Wang Q, Zhang J Q, Ma P C, Yao C M and Feng M 2015 *Phys. Rev. A* **91** 063827
[23] Djorwe P, Pennec Y and Djafari-Rouhani B 2019 *Phys. Rev. Appl.* **12** 024002
[24] Qiu L, Gan L, Ding W and Li Z Y 2013 *J. Opt. Soc. Am. B* **30** 1683
[25] Kepesidis K V, Bennett S D, Portolan S, Lukin M D and Rabl P 2013 *Phys. Rev. B* **88** 064105
[26] Genes C, Ritsch H, Drewsen M and Dantan A 2011 *Phys. Rev. A* **84** 051801
[27] Rossi M, Kralj N, Zippilli S, Natali R, Borrielli A, Pandraud G, Serra E, Di Giuseppe G and Vitali D 2017 *Phys. Rev. Lett.* **119** 123603
[28] Liu Y C, Xiao Y F, Luan X, Gong Q and Wong C W 2015 *Phys. Rev. A* **91** 033818
[29] Lai D G, Zou F, Hou B P, Xiao Y F and Liao J Q 2018 *Phys. Rev. A* **98** 023860
[30] Wilson-Rae I, Nooshi N, Zwerger W and Kippenberg T J 2007 *Phys. Rev. Lett.* **99** 093901
[31] Schliesser A, Rivière R, Anetsberger G, Arcizet O and Kippenberg T J 2007 *Nat. Phys.* **4** 415
[32] Chen X, Liu Y C, Peng P, Zhi Y and Xiao Y F 2015 *Phys. Rev. A* **92** 033841
[33] O'Connell A D, Hofheinz M, Ansmann M, Bialczak R C, Lenander M, Lucero E, Neeley M, Sank D, Wang H, Weides M, Wenner J, Martinis J M and Cleland A N 2010 *Nature* **464** 697
[34] Liu Y L and Liu Y X 2017 *Phys. Rev. A* **96** 023812

[35] Safavi-Naeini A H, Chan J, Hill J T, Alegre T P M, Krause A and Painter O 2012 *Phys. Rev. Lett.* **108** 033602
[36] Rossi M, Mason D, Chen J, Tsaturyan Y and Schliesser A 2018 *Nature* **563** 53
[37] Teufel J, Donner T, Li D, Harlow J, Allman M, Cicak K, Sirois A, Whittaker J, Lehnert K and Simmonds R 2011 *Nature* **475** 359
[38] Breyer D and Bienert M 2012 *Phys. Rev. A* **86** 053819
[39] Guo Y, Li K, Nie W and Li Y 2014 *Phys. Rev. A* **90** 053841
[40] Genes C, Ritsch H and Vitali D 2009 *Phys. Rev. A* **80** 061803
[41] Gu W j and Li G x 2013 *Phys. Rev. A* **87** 025804
[42] Huang J, Lai D G, Liu C, Huang J F, Nori F and Liao J Q 2022 *Phys. Rev. A* **106** 013526
[43] Liao Q H, Dai Y Z, Nie W J, Liu X and Liu Y C 2020 *J. Phys. B: At., Mol. Opt. Phys.* **53** 085402
[44] Bhattacharya M, Giscard P L and Meystre P 2008 *Phys. Rev. A* **77** 030303
[45] Chen Z, Peng J X, Fu J J and Feng X L 2019 *Opt. Express* **27** 29479
[46] Wang F, Shen K and Xu J 2023 *New J. Phys.* **24** 123044
[47] Peng J X, Chen Z, Yuan Q Z and Feng X L 2019 *Phys. Rev. A* **99** 043817
[48] Xiong H, Huang Y M and Wu Y 2021 *Phys. Rev. A* **103** 043506
[49] Bhattacharya M and Meystre P 2007 *Phys. Rev. Lett.* **99** 153603
[50] Cao X, Huang S, Deng L and Chen A 2024 *Photonics* **11** 960
[51] Liu Y M, Bai C H, Wang D Y, Wang T, Zheng M H, Wang H F, Zhu A D and Zhang S 2018 *Opt. Express* **26** 6143
[52] Wei D Z, Chen P C, Zhang Y P, Yao W Z, Ni R, Hu X P, Lv X J, Zhu S N, Xiao M and Zhang Y 2023 *Adv. Photon. Nexus* **2** 036007
[53] Oemrawsingh S S R, Eliel E R, Woerdman J P, Verstegen E J K, Kloosterboer J G and 't Hooft G W 2004 *J. Opt. A: Pure Appl. Opt.* **6** S288
[54] Volpe G and Petrov D 2006 *Phys. Rev. Lett.* **97** 210603
[55] Andersen M F, Ryu C, Cladé P, Natarajan V, Vaziri A, Helmerson K and Phillips W D 2006 *Phys. Rev. Lett.* **97** 170406
[56] Abdi M, Barzanjeh S, Tombesi P and Vitali D 2011 *Phys. Rev. A* **84** 032325
[57] Chen Y, Huang S, Deng L and Chen A 2024 *Opt. Express* **32** 17433
[58] Wang J, Zhang Q and Jing H 2024 *Phys. Rev. A* **110** 033505
[59] Pontin A, Biancofiore C, Serra E, Borrielli A, Cataliotti F S, Marino F, Prodi G A, Bonaldi M, Marin F and Vitali D 2014 *Phys. Rev. A* **89** 033810
[60] Zeng Y, Xiong B and Li C 2021 *Frontiers of Physics* **17** 12503
[61] Parniak M, Galinskiy I, Zwettler T and Polzik E S 2021 *Opt. Express* **29** 6935
[62] Safavi-Naeini A H, Chan J, Hill J T, Gröblacher S, Miao H, Chen Y, Aspelmeyer M and Painter O 2013 *New J. Phys.* **15** 035007
[63] Bhattacharya M, Giscard P L and Meystre P 2008 *Phys. Rev. A* **77** 013827
[64] He L, Liu Y X, Yi S, Sun C P and Nori F 2007 *Phys. Rev. A* **75** 063818
[65] Marquardt F, Chen J P, Clerk A A and Girvin S M 2007 *Phys. Rev. Lett.* **99** 093902
[66] Clerk A A, Devoret M H, Girvin S M, Marquardt F and Schoelkopf R J 2010 *Rev. Mod. Phys.* **82** 1155
[67] Mansouri D, Rezaie B, Ranjbar N A and Daeichian A 2023 *Phys. Scr.* **98** 105115
[68] Wang F and Gou C 2023 *Opt. Lett.* **48** 1164
[69] Shen Y, Campbell G T, Hage B, Zou H, Buchler B C and Lam P K 2013 *J. Opt.* **15** 044005
[70] Kleckner D and Bouwmeester D 2006 *Nature* **444** 75